Shock Formation and Breaking in Granular Avalanches

M. Shearer and N. Giffen
Department of Mathematics, North Carolina State University

October 29, 2009

Abstract

In this paper, we explore properties of shock wave solutions of the Gray-Thornton model for particle size segregation in granular avalanches. The model equation is a nonlinear scalar conservation law expressing conservation of mass under shear for the concentration of small particles in a bidisperse mixture. Shock waves are weak solutions of the partial differential equation across which the concentration jumps. We give precise criteria on smooth initial conditions under which a shock wave forms in the interior of the avalanche in finite time. Shocks typically lose stability as they are sheared by the flow, giving way to a complex structure in which a two-dimensional rarefaction wave interacts dynamically with a pair of shocks. The rarefaction represents a mixing zone, in which small and large particles are mixed as they are transported up and down (respectively) through the zone. The mixing zone expands and twice changes its detailed structure before reaching the boundary.

1 Introduction

In a dense, dry granular avalanche, larger grains are transported towards the upper free surface of the flow, and finer particles migrate towards the base. This process occurs throughout the natural world in debris flows, pyroclastic flows, as well as rock, sand, and snow avalanches. Particle-size segregation also arises in engineering and industrial applications such as the transport and processing of minerals, pharmaceuticals, and certain foods. The process of size segregation is thought to involve the combined effects of kinetic sieving, where smaller particles have a tendency to make their way downward through the gaps beneath them, and squeeze expulsion, where the larger particles are forced upward toward the free surface [10].

In this paper we obtain fundamental results concerning properties of the model of Gray and Thornton [4], a first order scalar conservation law describing the evolution of the volume fraction φ of small particles. The main results concern the tendency of a smooth distribution of particles to develop sharp interfaces across which the volume fraction φ jumps. In reality, diffusive remixing of particles smooths out the discontinuities [2], yet in slow, dry, frictional flows, Savage and Lun [10] still observed evidence of a sharp interface in chute experiments. For the Gray-Thornton model, we give criteria for the formation of shock waves in two-dimensional flow, using a procedure introduced by Lax [6], and employed on multidimensional conservation laws by Conway [1, 7]. However, the analysis is more subtle here due to shear within the flow, generating non-constant coefficients in the PDE. The Gray-Thornton model is just simple enough that a complete characterization of shock formation is possible.

Shear also causes certain shock wave solutions of the conservation law to lose stability [12]. Once a shock loses stability, the subsequent evolution is quite intricate; it has been explained in a special case resembling a two-dimensional Riemann problem [9], for which an explicit solution can be formulated that persists for a short time. In this paper, we show a simpler solution that evolves from more general initial conditions. However, this simpler solution appears only very briefly, after which, we track numerically the evolution of two-dimensional rarefaction waves that interact dynamically with shocks to form a persistent mixing zone.

The Gray-Thornton model is a scalar PDE for the evolution of the volume fraction, $\varphi(x, z, t)$, of small particles at a location (x, z) for each time t, where the x-axis is oriented in the direction of the avalanche

flow, and the z-axis is normal to the flow in the direction of the free surface. In this paper, we assume that there is no dependence on the transverse spatial variable y :

$$\varphi_t + u(z)\varphi_x + f(\varphi)_z = 0, \qquad -\infty < x < \infty,\ -1 < z < 1,\ t > 0. \tag{1.1}$$

As in [4], we assume that the given parallel bulk velocity $u(z)$, is time-independent and approximately linear, corresponding to a roughly constant shear rate within the avalanche:

In (1.1), the smooth function $f : [0, 1] \to \mathbb{R}$ is strictly convex and satisfies

$$f(0) = 0 = f(1); \tag{1.2}$$

it represents the flux of small particles in the normal direction due to size segregation. Correspondingly, $f(\varphi)/\varphi < 0$ is the speed of small particles in the z direction. In the original Gray-Thornton model, $f(\varphi) = S_r\varphi(\varphi - 1)$, so that the speed of small particles is controlled by the availability of large voids created by large particles as they roll and slide over other particles. The speed is reasonably taken to be proportional to $1-\varphi$, the volume fraction of large particles, with positive constant of proportionality S_r setting the segregation rate. This form for $f(\varphi)$ is justified in [4] using mixture theory, in which the motion of an individual particle is governed by net forces due to gravity, squeeze expulsion, and friction with other particles, the latter being identified with the Stokes drag of a viscous fluid on a sphere. In this paper, we also consider more general smooth convex functions $f(\varphi)$.

While it would be possible in principle to couple the mass conservation equation (1.1) to an equation for the location of the free surface, it is simpler to assume the flow is sufficiently well developed that we can take the free surface height to be constant; for our purposes, we have normalized the height so that $-1 \le z \le 1$. In particular, this precludes consideration of interesting issues near the front of the avalanche (but see [14] for a steady flow with recirculation and segregation).

In Section 2, we describe properties of the PDE (1.1), including equations for characteristics and shock waves, and a discussion of shock wave stability. In Section 3, we give a characterization of initial conditions for which the solution develops interior shock waves in finite time. The analytical results are demonstrated with numerical simulations performed with a simple finite difference method. In Section 4, we analyze solutions immediately after a shock breaks down (i.e., loses stability) at a single location. The solution involves a small zone in which small and large particles are mixed. After a short time, this zone develops a shock wave on part of its boundary. In Section 5, we track the subsequent evolution numerically, identifying two slightly different stages in the structure of the solution.

2 Characteristics and shocks

In this section, we outline basic properties of the PDE (1.1) that are used to construct and analyze solutions in subsequent sections. We describe characteristic surfaces and shock waves, together with shock wave stability.

2.1 Characteristics

Equation (1.1) is a scalar equation in conservation form, so the theory of scalar conservation laws can be applied to construct solutions. Characteristics $x = x(t), z = z(t)$ are curves along which the solution φ is constant. A characteristic curve passing through a point (x_0, z_0) at time $t = t_0$ satisfies the initial value problem

$$\frac{dx}{dt} = u(z); \quad \frac{dz}{dt} = f'(\varphi); \quad x(t_0) = x_0;\ z(t_0) = z_0. \tag{2.1}$$

The system is solved easily for general non-negative $u(z)$, since t may be eliminated:

$$u(z)\frac{dz}{dx} = f'(\varphi).$$

Since φ is constant on characteristics, if we let

$$\psi(z) = \int_0^z u(\zeta)\, d\zeta, \tag{2.2}$$

we obtain x as a function of z :

$$\psi(z) - \psi(z_0) = f'(\varphi)(x - x_0). \tag{2.3}$$

In the particular case $f(\varphi) = \varphi(\varphi - 1)$, this gives an equation for φ along each characteristic:

$$\varphi = \frac{1}{2}\left(1 + \frac{\psi(z) - \psi(z_0)}{x - x_0}\right). \tag{2.4}$$

More generally, integrating (2.1), we obtain

$$x(t) = \int_{t_0}^t u(z(t))\, dt + x_0, \quad z(t) = f'(\varphi)(t - t_0) + z_0, \tag{2.5}$$

In the special case of linear $u(z)$, characteristic curves are parabolic in space-time. Specifically, for $u(z) = z$,

$$x(t; t_0) = \tfrac{1}{2} f'(\varphi)(t - t_0)^2 + z_0(t - t_0) + x_0, \quad z(t; t_0) = f'(\varphi)(t - t_0) + z_0, \tag{2.6}$$

where for each t and each φ, (2.6) is a contour of φ parameterized by t_0.

2.2 Shock waves

A shock wave solution of equation (1.1) is a weak solution of the PDE in which $\varphi(x, z, t)$ is discontinuous across an interface, represented by a curve $z = \hat{z}(x, t)$. Since equation (1.1) is in conservation form, we can write the Rankine-Hugoniot condition relating the normal speed of a shock wave to the jump in φ and the flux of φ across the wave:

$$\hat{z}_t[\varphi] + u(\hat{z})\hat{z}_x[\varphi] + [f(\varphi)] = 0. \tag{2.7}$$

Here, square brackets indicate the jump, i.e., the difference between left and right-hand limits: $[v] = v_+ - v_-$. Let $\varphi_\pm(x, t) = \varphi(x, \hat{z}(x, t)\pm, t)$ denote the one-sided limits of φ. Dividing by $[\varphi]$, equation (2.7) becomes (dropping the hats):

$$z_t + u(z)z_x = G(\varphi_+, \varphi_-), \quad G(\eta, \nu) = \frac{f(\eta) - f(\nu)}{\eta - \nu}, \eta \neq \nu,\ G(\eta, \eta) = f'(\eta). \tag{2.8}$$

This equation is a nonlinear PDE, a conservation law with source terms. In general, it is coupled to the solution φ, but if φ is known, then the PDE determines the evolution of the interface $z = \hat{z}(x, t)$ directly.

We have the following theorem that states a shock wave is stable (in the sense of hyperbolic PDE [11]) if there is a greater density of large particles above the interface than below. The result was proved in [12] in the special case of quadratic $f(\varphi)$. Let $z = \hat{z}(x, t)$ be a smooth interface with $\varphi_\pm(x, t) = \varphi(x, z(x, t)\pm, t)$.

Theorem 2.1 *The interface $z = \hat{z}(x, t)$ is dynamically stable if $\varphi_+ < \varphi_-$; it is unstable if $\varphi_+ > \varphi_-$.*

Proof: We need to show that surfaces of characteristics from each side of the shock overlap, so that the shock location can be determined between the characteristic surfaces. We do this by calculating speeds of the characteristics and shock normal to the shock wave at a given time $t = t_0$.

Suppose $z = \hat{z}(x_0, t_0)$ is the shock $\mathcal{S}$ at time $t = t_0$, the curve being parameterized by x_0. Let characteristics originating at $(x, z) = (x_0, \hat{z}(x_0, t_0))$ with $\varphi = \varphi_\pm$ be denoted $x_\pm(t; x_0), z_\pm(t; x_0), t > t_0$, forming characteristic surfaces. From each $(x_0, z_0) \in \mathcal{S}$, we calculate the normal component of the tangents $\partial_t(x_\pm(t; x_0), z_\pm(t; x_0))$ at $t = t_0$:

$$\frac{1}{\sqrt{1 + \hat{z}_x^2}}(-\hat{z}_x, 1) \cdot (u(\hat{z}), f'(\varphi_\pm)), \tag{2.9}$$

using the ODE for the characteristics. A similar calculation for the shock surface $(x, \hat{z}(x,t), t)$ yields the speed in the normal direction:

$$\frac{1}{\sqrt{1+\hat{z}_x^2}}(-\hat{z}_x, 1)\cdot(0, -u(\hat{z})\hat{z}_x + G(\varphi_+, \varphi_-)), \tag{2.10}$$

where we have used the PDE (2.8). But for $\varphi_+ < \varphi_-$, since f is a convex function, we have $f'(\varphi_+) < G(\varphi_+, \varphi_-) < f'(\varphi_-)$, with each of the inequalities reversed if $\varphi_+ > \varphi_-$. Comparing speeds (2.9),(2.10) completes the proof. ■

3 Shock Formation

The formation of shock waves in nonlinear hyperbolic systems is well documented in one space dimension [5], but in multiple dimensions, the analysis is largely confined to scalar equations [7]. In this section, we consider initial value problems

$$\varphi_t + u(z)\varphi_x + f(\varphi)_z = 0, \quad -\infty < x, z < \infty,\ t > 0 \tag{3.1a}$$

$$\varphi(x, z, 0) = \varphi_0(x, z) \quad -\infty < x, z < \infty, \tag{3.1b}$$

and characterize initial data φ_0 from which shocks form in finite time. Since solutions of scalar conservation laws remain bounded, the signature of shock formation is a singularity in the solution involving the gradient becoming unbounded. For a nonlinear scalar equation in multiple space dimensions, with constant coefficients, the magnitude of the gradient evolves according to a simple Ricatti equation, as explained in [7]. However, for equation (3.1a), the evolution is more complicated due to the non-constant coefficient induced by shear.

In practice, shock waves also form at the horizontal boundaries $z = \pm 1$ (and can be introduced through lateral boundaries as well). Physically, a layer of large particles (for which $\varphi = 0$) develops at $z = 1$ as soon as the first large particle reaches that boundary, and similarly a layer of small particles (with $\varphi = 1$) develops at the lower boundary $z = -1$. Such a layer can be part of a region in which $\varphi(x, z, t)$ remains continuous, but only if there is a layer already present in the initial condition.

3.1 Analysis of interior shock formation

First, we analyze shock formation in the interior of the domain. Differentiating equation (3.1a) successively with respect to x and z, we obtain a system of equations for $(\varphi_x, \varphi_z) = (v, w)$:

$$\frac{dv}{dt} = -f''(\varphi)vw \tag{3.2a}$$

$$\frac{dw}{dt} = -u'(z)v - f''(\varphi)w^2. \tag{3.2b}$$

Here, $\frac{d}{dt} = \partial_t + u(z)\partial_x + f'(\varphi)\partial_z$ is differentiation along a characteristic (2.1), on which φ is constant, and z is a linear function of t, as in (2.5). Thus, system (3.2) is autonomous precisely in the case of simple shear, for which $u(z)$ is linear. If so, the positive constants u' and $f''(\varphi)$ can be scaled out of the system, and we consider the specific case $u(z) = z, f(\varphi) = \varphi(\varphi - 1)$. This gives the ODE system for $\nabla\varphi = (v, w)$:

$$\frac{dv}{dt} = -2vw \tag{3.3a}$$

$$\frac{dw}{dt} = -v - 2w^2. \tag{3.3b}$$

We observe the following properties of system (3.3):

(1) The system has a first integral: solution trajectories lie on the conic sections

$$w^2 + \kappa v^2 + v = 0, \tag{3.4}$$

where κ is constant. The curves are ellipses for $\kappa > 0$, and hyperbolas for $\kappa < 0$; the curve $v = -w^2$ for $\kappa = 0$ is a parabola. The (v, w) phase portrait shown in Fig. 3.1.

(2) The system is invariant under $t \to t/\alpha, v \to \alpha^2 v, w \to \alpha w$ for any $\alpha \neq 0$. In particular (with $\alpha = -1$), $w(t)$ is odd, and $v(t)$ is even, if $w(0) = 0$.

(3) The solution of (3.3) with initial conditions $v(0) = v_0, w(0) = w_0$, is

$$v(t) = \frac{v_0}{q(t)}, \quad w(t) = \frac{w_0 - v_0 t}{q(t)}, \quad q(t) = 1 + 2w_0 t - v_0 t^2. \tag{3.5}$$

The zeros of $q(t)$ are

$$t_\pm(v_0, w_0) = \begin{cases} \dfrac{w_0}{v_0} \pm \dfrac{1}{v_0}\sqrt{w_0^2 + v_0}, & \text{if } v_0 \neq 0 \\ -\dfrac{1}{2w_0} & \text{if } v_0 = 0, w_0 \neq 0. \end{cases} \tag{3.6}$$

Consequently, we have the following cases.

(a) If $v_0 > 0$, then $t_- < 0 < t_+$.

(b) If $-w_0^2 \leq v_0 \leq 0$, and $w_0 < 0$ then $0 < t_+ \leq t_-$.

(c) If $-w_0^2 \leq v_0 \leq 0$, and $w_0 > 0$, then $t_\pm < 0$.

(d) If $v_0 < -w_0^2$, then $t_\pm$ are complex.

Therefore, all the trajectories in the phase portrait that are unbounded in forward time involve finite time blow-up of $\nabla\varphi = (v, w)$, i.e., cases (a), (b). Trajectories that are bounded, i.e., cases (c), (d), have algebraic decay to the origin as $t \to \infty$. Since the blow-up of $\nabla\varphi$ on characteristics is governed by these solutions, we can give precise conclusions for shock formation based on the gradient of the initial data. Let Γ be the union of the curve $\{(v_0, w_0) : v_0 = -w_0^2, w_0 < 0\}$ with the positive w_0 axis: $\{(0, w_0) : w_0 \geq 0\}$, and let $\mathcal{D}$ denote the region to the right of Γ in the (v, w) plane, i.e., with $v > 0$, or $-w^2 \leq v \leq 0$, and $w < 0$. Consider the initial value problem on the entire plane:

$$\varphi_t + z\varphi_x + (\varphi(\varphi - 1))_z = 0, \quad -\infty < x, z < \infty, \ t > 0 \tag{3.7a}$$

$$\varphi(x, z, 0) = \varphi_0(x, z) \quad -\infty < x, z < \infty. \tag{3.7b}$$

Theorem 3.1 *Let $\varphi_0 \in C^1(\mathbb{R}^2)$, with $0 \leq \varphi_0(x, z) \leq 1$ for all $(x, z) \in \mathbb{R}^2$. If $\nabla\varphi_0(x, z) = (v_0, w_0)$ lies in $\mathcal{D}$ for any (x, z), then the solution $\varphi(x, z, t)$ of the initial value problem (3.7) develops a singularity: $\sup_{(x,z)} |\nabla\varphi(x, z, t)| \to \infty$ as $t \to t^*-$ in finite time t^* given by*

$$t^* = \inf\{t_+(\nabla\varphi_0(x, z)) : \nabla\varphi_0(x, z) \in \mathcal{D}\} \tag{3.8}$$

Proof: If $(v_0, w_0) \in \mathcal{D}$, then $t_+ > 0$ is real, and t_- is either negative or greater than t_+. Individual contours evolve according to (2.1), and the normal $(v, w) = \nabla\varphi$ evolves along characteristic curves (on which φ is

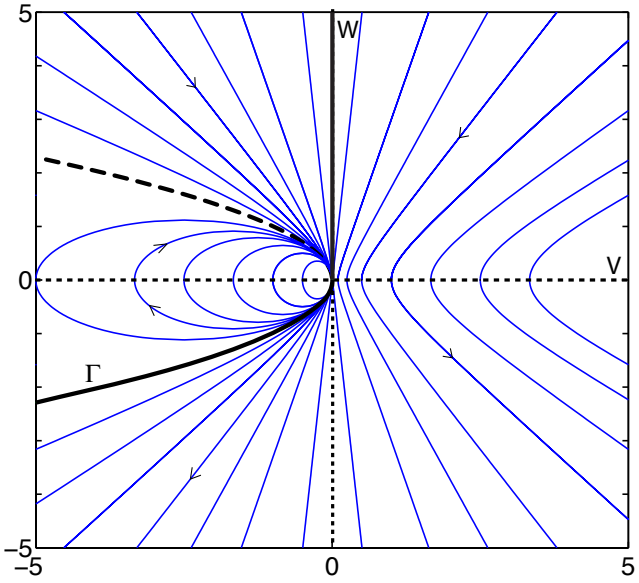

Figure 3.1: The phase portrait for system (3.3).

constant) according to (3.3). Consequently, the singularity $|\nabla\varphi| \to \infty$ develops at the smallest value of t_+, evaluated on the initial data, as in (3.8). ■

We interpret the theorem by dividing the region $\mathcal{D}$ and its complement in the (v_0, w_0) plane into regions in which the behavior of the characteristics can be determined in detail.

(i) $v_0 > 0, w_0 > 0$. In this case, the trajectory lies on the hyperbola (3.4) with $\kappa = \kappa_0 < 0$ given by $w_0^2 + \kappa_0 v_0^2 + v_0 = 0$. The phase portrait Fig.3.1 shows that $|\nabla\varphi| = |(v, w)|$ decreases, corresponding to contours of φ becoming more spread out, until the trajectory crosses the v-axis. From (3.5), we see that this occurs at time $t = w_0/v_0$, when the contour of φ becomes vertical at this point (x, z). Subsequently, $\nabla\varphi = (v, w)$ lies in the fourth quadrant $v > 0, w < 0$, so that the contour has positive slope in the (x, z)-plane. In this quadrant, $|\nabla\varphi| = |(v, w)|$ increases, so that contours are getting closer. Then $v(t)$ and $w(t)$ blow up in finite time, the time given by the positive zero of $q(t)$ in (3.6):

$$t_+ = \frac{w_0}{v_0} + \frac{1}{v_0}\sqrt{w_0^2 + v_0}. \tag{3.9}$$

At this time, the solution $\varphi(x, z, t)$ develops a discontinuity at this value of (x, z).

(ii) $v_0 > 0, w_0 < 0$. As discussed under case (i), $|\nabla\varphi| = |(v, w)|$ increases, and blows up at time (3.9).

Cases (i) and (ii) in summary show that $|\nabla\varphi| \to \infty$ along the characteristic as $t \to \infty$ if $\varphi_x > 0$ initially. Physically, the contour eventually has a mix of more small particles below a mix with more large particles; subsequent segregation sharpens the profile of φ until a shock forms.

(iii) $-w_0^2 < v_0 < 0, w_0 < 0$. In this case, the trajectory lies on the hyperbola (3.4) with $\kappa = \kappa_0 < 0$ given by $w_0^2 + \kappa_0 v_0^2 + v_0 = 0$, but in the third quadrant since $v_0 < 0$. Once again, $|\nabla\varphi| = |(v, w)|$ increases, with the blowup time given by t_+, the smaller of the two positive zeros of $q(t)$ in (3.6). In contrast to cases (i) and (ii), the contours in case (iii) continue to have positive (but decreasing) slope as they get closer together and eventually form a shock.

(iv) In the remaining cases, for which $w_0 > -\sqrt{-v_0}, v_0 < 0$, the contour may switch from having negative slope (if $w_0 < 0$) to positive slope (with $w > 0$), in which case, $|\nabla\varphi|$ increases before decreasing to zero. That is, contours compress before expanding. But if $w_0 > 0$, then $|\nabla\varphi|$ decreases monotonically to zero; the contours start expanding immediately and never compress.

3.2 Simulations

In this subsection we illustrate the results of subsection §3.1 with numerical simulations. The finite difference code employs an explicit time step, upwind differencing in x, and a first order Godunov method in the z-direction. The computational domain is $-3 < x < 3,\ -1 < z < 1$, and results are plotted on the smaller domain $-1 < x < 1,\ -1 < z < 1$ over a time short enough that the effects of the lateral boundaries $x = \pm 3$ are not observed. Boundary conditions at $z = \pm 1$ require that particles do not penetrate the boundaries:

$$\varphi(x, -1) = 1, \quad \varphi(x, 1) = 0. \tag{3.10}$$

While these boundary conditions are consistent with no-flux boundary conditions $f(\varphi) = 0$, they are easier to impose in the numerical code. In fact, with boundary conditions (3.10), if $\varphi = 0$ next to $z = -1$ (or respectively, $\varphi = 1$ next to $z = 1$), then there is a horizontal stationary shock at that boundary location. The shock remains horizontal and stationary until small particles reach the bottom $z = -1$ (or, respectively, large particles reach the top $z = 1$). In the simulations, we choose initial data

$$\varphi_0(x, z) = \pm 0.1 \tan\left(\frac{\pi}{2} z\right) + \frac{1}{2} \pm x, \tag{3.11}$$

giving four cases in all. These four examples illustrate all the features of shock formation, since

$$\nabla\varphi_0 = (v_0, w_0) = \left(\pm 1, \pm 0.1 \frac{\pi}{2} \sec^2\left(\frac{\pi}{2} z\right)\right) \tag{3.12}$$

can be placed in each of the four cases (i-iv) of §3.1.

In Fig. 3.2, $\nabla\varphi_0 = (v_0, w_0)$ is in the first quadrant, so that to start with, contours of φ spread out, while steepening as the normal $\nabla\varphi$ rotates clockwise. As the contours reach the boundaries $z = \pm 1$, a layer of small particles grows from $z = -1$, with a sharp shock wave interface propagating upwards. Similarly, a layer of large particles grows from $z = 1$, led by a shock wave propagating downwards. Between these shocks, contours continue to rotate until their normals eventually enter the fourth quadrant. Using (3.12), we calculate that this occurs at $z = 0, t \approx 0.157$. Subsequently the interior contours compress where they have positive slope, with a corresponding steepening of the graph of φ. By time $t = 1.3$ an interior shock has formed. This is in agreement with the prediction of Theorem 3.1, which from (3.12), gives a shock formation time $t^* \approx 1.169$.

In Fig. 3.3, $\nabla\varphi_0 = (v_0, w_0)$ is in the fourth quadrant everywhere it is non-zero. Consequently, an interior shock forms quickly, where the gradient is steepest, which happens to be at the edges $x = \pm 1$ in these simulations. The shock then propagates towards the center of the domain, leading to full segregation by time $t = 0.8$.

In Fig. 3.4, $\nabla\varphi_0 = (v_0, w_0)$ is in the second quadrant everywhere, and contours rotate and spread out as $\nabla\varphi$ proceeds along a trajectory to the origin. Contours near the upper and lower boundaries quickly touch the boundaries, generating layers of small and large particles. The only shocks in this solution form the boundaries of these layers.

In Fig. 3.5, $\nabla\varphi_0 = (v_0, w_0)$ is in the third quadrant everywhere; it is closer to vertical, i.e., outside the parabola $v_0 = -w_0^2$, towards the lateral boundaries $x = \pm 1$. In these regions, the gradient quickly blows up, yielding a shock. Portions of the contours where the gradient is initially inside the parabola evolve with rotation, with the contours spreading as the gradient approaches the origin after crossing the horizontal axis (where the contours become vertical). The subsequent evolution consists of a pair of shocks trapping a central region in which small and large particles are mixed.

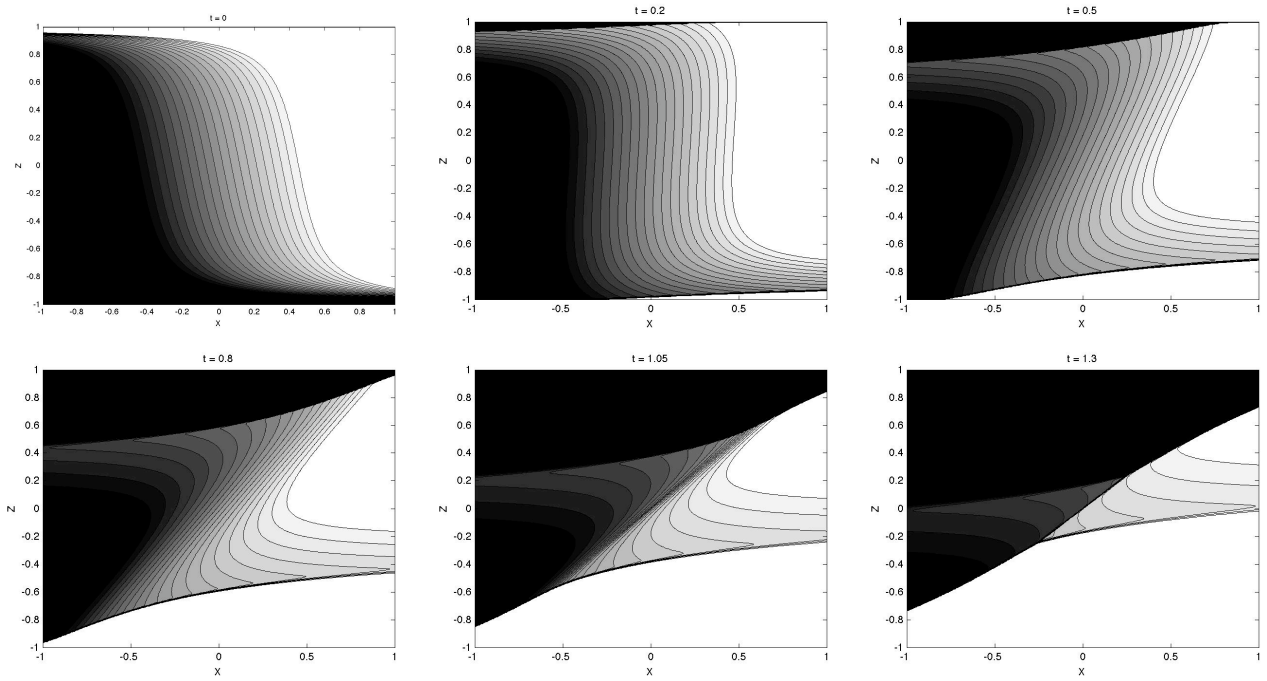

Figure 3.2: Shock formation from initial data φ_0 with $\nabla\varphi_0$ in the first quadrant.

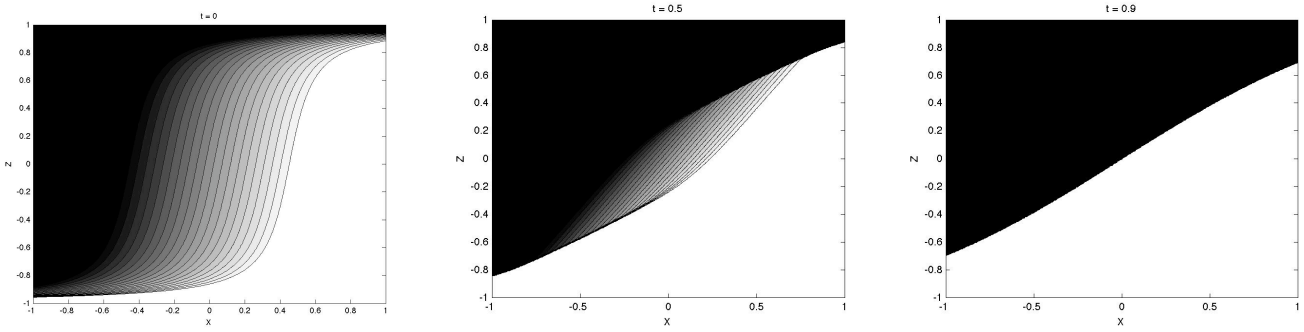

Figure 3.3: Shock formation from initial data φ_0 with $\nabla\varphi_0$ in the fourth quadrant.

4 Shock Breaking

In this section we consider a shock wave $z = \hat{z}(x,t)$ that separates two constant values of φ. The evolution of the interface is governed by the nonlinear PDE (2.8). If the shock is stable and decreasing, in that $\hat{z}_x < 0$, then the shock tends to steepen and break, due to shear. That is, $\min_x \hat{z}_x(x,t) \to -\infty$ in finite time. The tangent first becomes vertical at an inflection point. Subsequently, the interface could evolve according to the Rankine-Hugoniot condition, for example by expressing x as a function of z, t. However, the resulting piecewise constant solution is unstable because in this weak solution of the PDE (3.1a), part of the evolved shock wave is unstable according to Theorem 2.1. The stable solution that we construct in §4.1 replaces the central unstable section with a continuous wave constructed by the method of characteristics. This

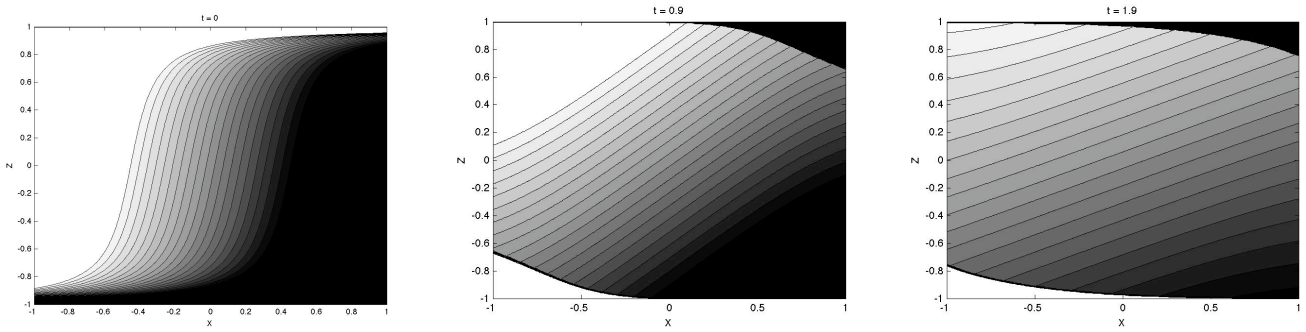

Figure 3.4: The absence of interior shock formation from initial data φ_0 with $\nabla\varphi_0$ in the second quadrant.

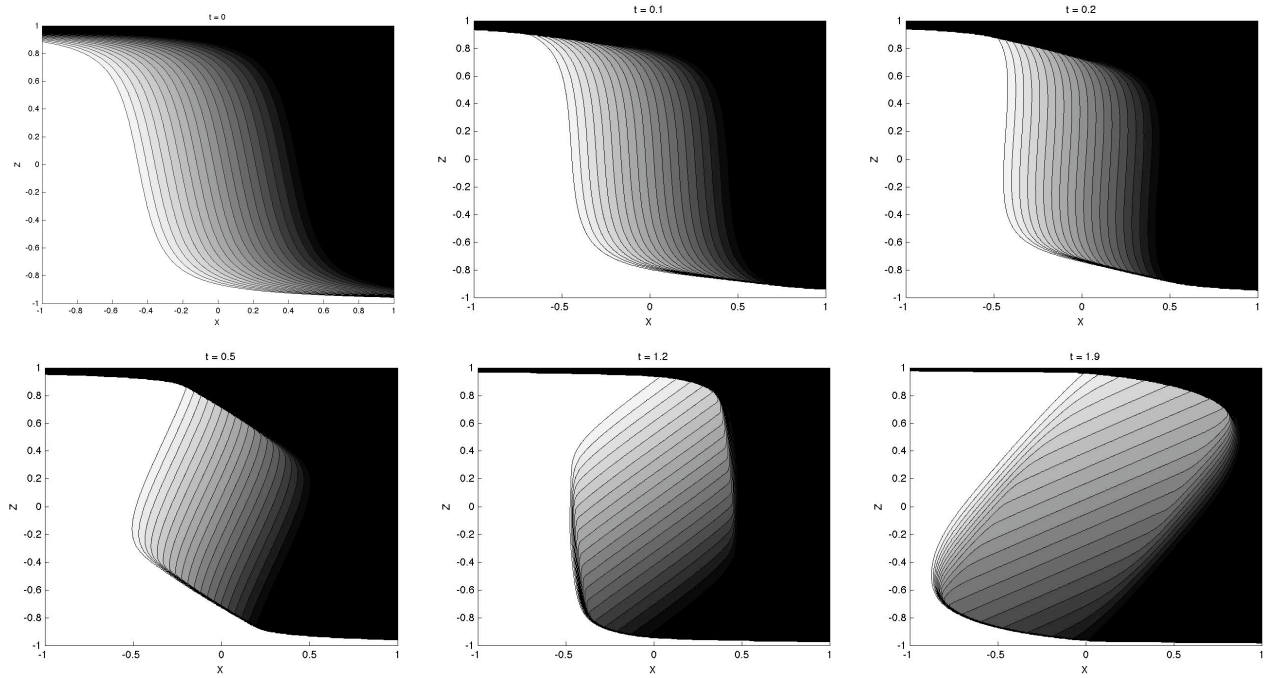

Figure 3.5: Shock formation from initial data φ_0 with $\nabla\varphi_0$ in the third quadrant.

solution, consisting of stable parts of the evolved shock, and a central mixing zone across which φ varies continuously from φ_- to φ_+, persists typically only for a short time, after which the stable portion of the evolved shock is affected by the mixing zone. (We also consider a special case in which this simple structure persists indefinitely.) The subsequent evolution of the stable solution is more complicated, and undergoes another change before settling down to a final form. The latter stages are described in § 5, and verified with numerical simulation.

In this section, we consider the initial value problem (3.7). It is instructive to look first at the simple case of a vertical initial interface $x = 0$; the following construction forms part of the solution of an initial

boundary value problem in [9]. Accordingly, we consider an initial condition

$$\varphi(x,z,0) = \varphi_0(x,z) = \begin{cases} \varphi_-, & \text{if } x < 0 \\ \\ \varphi_+, & \text{if } x > 0 \end{cases} \tag{4.1}$$

It is convenient to track the interface in the form $x = x(z,t)$, which evolves according to the Rankine-Hugoniot condition, i.e.,

$$x_t + r x_z = z, \quad r = \varphi_- + \varphi_+ - 1, \tag{4.2}$$

with initial condition

$$x(z,0) = 0. \tag{4.3}$$

Solving (4.2), (4.3), we find

$$x(z,t) = zt - \tfrac{1}{2} r t^2, \quad t \geq 0. \tag{4.4}$$

Thus, if $\varphi_- < \varphi_+$, then the interface (4.4) evolves maintaining stability, with φ_- above the larger φ_+, since $\partial x/\partial z = t > 0$.

On the other hand, if $\varphi_- > \varphi_+$, then the evolved interface (4.4) is unstable, and the stable solution is a rarefaction wave that continues to shear:

$$\varphi(x,z,t) = \begin{cases} \varphi_-, & x < x_-(t) \\ \\ \dfrac{1}{2} - \dfrac{x - zt}{t^2}, & x_-(t) \leq x \leq x_+(t) \\ \\ \varphi_+, & x > x_+(t), \end{cases} \tag{4.5}$$

where $x_\pm(t) = zt - \frac{1}{2}(2\varphi_\pm - 1)t^2$.

Now we turn to the more general situation, in which we consider (3.7) with an initial condition that has a shock or sharp interface $x = g(z)$ separating two constant values $\varphi_- > \varphi_+$ of φ:

$$\varphi(x,z,0) = \varphi_0(x,z) = \begin{cases} \varphi_-, & \text{if } x < g(z) \\ \\ \varphi_+, & \text{if } x > g(z). \end{cases} \tag{4.6}$$

For a general decreasing function $g(z)$, the shock will steepen and eventually break. Anticipating this finite time singularity, we take $g(z)$ to represent a shock on the verge of breaking at $z = 0$. Accordingly, we assume g is at least C^4, with

$$g(0) = 0, \ g'(0) = 0, \ g''(0) = 0, \ g'''(z) < 0 \ \text{ for all } \ z. \tag{4.7}$$

Then $g'(z) < 0$ and $z g''(z) < 0$ for all $z \neq 0$. In particular, the interface is initially vertical at $z = 0$, and decreasing elsewhere. As for the vertical interface, the interface $x = x(z,t)$ evolves according to the Rankine-Hugoniot condition, expressed by the PDE (4.2), with initial condition $x(z,0) = g(z)$, which we solve by the method of characteristics:

$$\frac{dx}{dt} = z, \qquad \frac{dz}{dt} = r, \quad x(0) = g(z_0); \ z(0) = z_0, \quad r = \varphi_- + \varphi_+ - 1. \tag{4.8}$$

Thus, characteristics are given by

$$x = \frac{1}{2} r t^2 + z_0 t + g(z_0); \quad z = rt + z_0. \tag{4.9}$$

Eliminating z_0, we have

$$x(z,t) = -\frac{1}{2} r t^2 + zt + g(z - rt), \tag{4.10}$$

which we shall refer to as *the evolved interface*. In particular, at $z = rt$, $\frac{\partial x}{\partial z} = t > 0$, so that the interface has positive slope over some middle portion, where φ_- is now above φ_+. Thus, this portion of the evolved interface is unstable.

4.1 The Mixing Zone

For fixed $t > 0$, the unstable portion of the evolved interface lies between the two extrema of the evolved interface (4.10), which we label $P_\pm(t) = (x_\pm(t), z_\pm(t))$. From (4.10) we find $z = z_\pm(t)$ satisfies

$$\frac{\partial}{\partial z} x(z,t) = t + g'(z - rt) = 0. \tag{4.11}$$

Since g' is concave, equation (4.11) has two solutions $z = z_\pm(t)$, with $z_-(t) < rt < z_+(t)$, for each $t > 0$. Then $x_\pm(t)$ is determined from (4.10) with $z = z_\pm(t)$. Moreover, differentiating this relation with respect to t, we calculate from (4.10) and (4.11)

$$x'_\pm(t) = z_\pm(t). \tag{4.12}$$

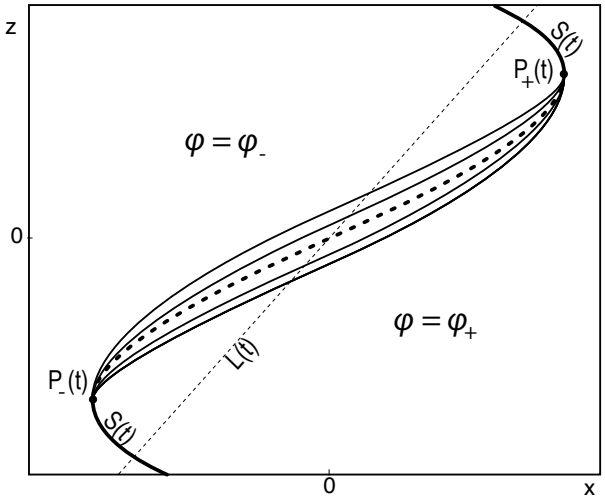

Figure 4.1: Schematic of the mixing zone joining constant values $\varphi_- > \varphi_+$. $S(t)$ is the stable part of the evolved interface; the dashed line is the unstable part, and also the contour $\varphi = \frac{1}{2}(\varphi_+ + \varphi_-)$.

Now we can construct the solution that replaces the evolved interface between the two extrema $P_\pm(t)$. In Fig. 4.1, we show the evolved interface $S(t)$ and contours $C^\pm_\varphi(t)$ of $\varphi(x,z,t)$, $\varphi_+ \le \varphi \le \varphi_-$, running between the two extrema $P_\pm(t)$ of the curve $S(t)$. The contours $C^\pm_\varphi(t)$ are given by the general form (2.6) with $f(\varphi) = \varphi(\varphi - 1)$, and initial points specified by $P_\pm(t_1) : x_0 = x_\pm(t_1), z_0 = z_\pm(t_1)$, where $t_1 \in [0,t]$ parameterizes the curve at fixed t. Thus,

$$C^\pm_\varphi(t) = \{(x^\pm(t,t_1,\varphi), z^\pm(t,t_1,\varphi)), \quad 0 \le t_1 \le t\}, \tag{4.13}$$

with

$$x^\pm(t,t_1,\varphi) = \frac{1}{2}(2\varphi - 1)(t - t_1)^2 + z_\pm(t_1)(t - t_1) + x_\pm(t_1), \quad z^\pm(t,t_1,\varphi) = (2\varphi - 1)(t - t_1) + z_\pm(t_1). \tag{4.14}$$

In particular, for $\varphi = \frac{1}{2}(\varphi_+ + \varphi_-)$, $C^\pm_\varphi(t)$ coincides with the evolved interface (4.10).

We shall use the following properties of the characteristics $C^\pm_\varphi(t)$, which are verified by differentiating (4.14) and using (4.11), (4.12).

- For each $t > 0$, the characteristics (4.14) all emanate from $P_\pm(t)$, when $t_1 = t$.

  I.e., $x^\pm(t,t,\varphi) = x_\pm(t)$; $z^\pm(t,t,\varphi) = z_\pm(t)$, for each $\varphi \in [\varphi_+, \varphi_-]$.

- Each $C^{\pm}_{\varphi}(t)$, ends, at $t_1 = 0$, on the same line $L(t) : x = \frac{1}{2}tz :\ x^{\pm}(t, 0, \varphi) = \frac{1}{2}tz^{\pm}(t, 0, \varphi)$.
- Each $C^{\pm}_{\varphi}(t)$ has the same slope at each $t_1 \in [0, t]$; in particular, they all terminate with the same slope $\dfrac{dx}{dz} = t$ on $L(t)$ (so that the characteristics have half the slope of $L(t)$ where they intersect the line).

Provided $z^+(t, t_1, \varphi)$ is an increasing function of $t_1 \in (0, t)$, and $z^-(t, t_1, \varphi)$ is decreasing in $t_1 \in (0, t)$, the characteristics $C^{\pm}_{\varphi}(t)$ form a mixing zone $\mathcal{M}_1(t)$ between $P_+(t)$ and $P_-(t)$, in which φ varies continuously from $\varphi = \varphi_-$ to $\varphi = \varphi_+$. The mixing zone has boundary consisting of the four curves $C^{\pm}_{\varphi_\pm}(t)$. Within $\mathcal{M}_1(t)$, the solution $\varphi(x, z, t)$ is defined implicitly from the equations

$$x = x^{\pm}(t, t_1, \varphi), \quad z = z^{\pm}(t, t_1, \varphi), \quad 0 < t_1 < t, \quad \varphi_+ < \varphi < \varphi_-. \tag{4.15}$$

Outside $\mathcal{M}_1(t)$, the solution $\varphi(x, z, t)$ is φ_- (to the left of $C^{\pm}_{\varphi_-}(t)$ and the evolved shock), and φ_+ (to the right of $C^{\pm}_{\varphi_+}(t)$ and the evolved shock). In what follows, we refer to this solution, illustrated at a fixed t in Fig. 4.1, as *the smooth mixing solution.*

Evolutionary Property. We claim that by construction, the smooth mixing solution is evolutionary. Indeed, each point of each characteristic at time $t > 0$ is evolved from a point $P_{\pm}(t_0)$ at an earlier time $t_0 \geq 0$. The curves $C^{\pm}_{\varphi}(t)$ are made up of such points, and are hence evolutionary. As a further check, we show that the mixing region $\mathcal{M}_1(t)$ relates properly to characteristics evolved from the initial condition. For $\varphi_+ \leq \varphi \leq \varphi_-$, and $t \geq 0$, let $S_\varphi(t)$ denote the curve obtained by evolving (x, z) along characteristics $\varphi =$ constant starting at points $(x_0 = g(z_0), z_0)$ on the initial interface:

$$S_\varphi(t): \quad \begin{cases} x_s(\varphi, t; z_0) = \dfrac{1}{2}(2\varphi - 1)t^2 + z_0 t + g(z_0) \\ \\ z_s(\varphi, t; z_0) = (2\varphi - 1)t + z_0 \end{cases} \tag{4.16}$$

Now consider all the characteristics $\varphi = \varphi_-$ evolving from the initial condition, i.e., with $x \leq g(z)$. The intersection of the characteristics with a plane $t =$ constant is a region in the (x, z) plane, bounded on the right by $S_{\varphi_-}(t)$. Similarly, the region $x \geq g(z)$, where $\varphi = \varphi_+$ initially, is evolved to a region bounded on the left by $S_{\varphi_+}(t)$. Any point (x, z) to the right of $S_{\varphi_-}(t)$ must have $\varphi(x, z, t) < \varphi_-$, if $\varphi(x, z, t)$ is the weak solution that is evolutionary, and any point to the left of $S_{\varphi_+}(t)$ must have $\varphi(x, z, t) > \varphi_+$. To check that $\mathcal{M}_1(t)$ is consistent with these observations, we verify that $C_{\varphi_+}(t)$ is to the right of $S_{\varphi_+}(t)$ for each $t > 0$. The argument that $C_{\varphi_-}(t)$ is to the left of $S_{\varphi_-}(t)$ is similar. First recall that points (x^+, z^+) on $C_{\varphi_+}(t)$ are given in (4.14). We wish to consider a point $(x_s, z_s) \in S_{\varphi_+}$ with the same value of z, and then we show $x^+ > x_s$. That is, to verify the evolutionary property of the smooth mixing solution, we prove:

Lemma 1 $z^+(t, t_1, \varphi_+) = z_s(\varphi_+, t, z_0)$ *implies* $x^+(t, t_1, \varphi_+) > x_s(\varphi_+, t, z_0)$.

Proof: Suppose

$$z^+(t, t_1, \varphi_+) = z_s(\varphi_+, t, z_0).$$

Then, from the definitions (4.14), (4.16) of z^+, z_s, we find

$$z_0 = z_+(t_1) - (2\varphi_+ - 1)t_1.$$

With this observation, we find, using equation (4.10) for $x_+(t)$, that

$$x^+(t, t_1, \varphi_+) - x_s(\varphi_+, t, z_0) = \frac{1}{2}(\varphi_+ - \varphi_-)t_1^2 + g(z_+(t_1) - (\varphi_+ + \varphi_- - 1)t_1) - g(z_+(t_1) - (2\varphi_+ - 1)t_1).$$

Now we use the definition $g'(z_+(t_1) - (\varphi_+ + \varphi_- - 1)t_1) = -t$, of z_+ to deduce that $z_+(t_1) - (\varphi_+ + \varphi_- - 1)t_1 > 0$ (since $g'(z) < 0$ if and only if $z > 0$). The Taylor expansion of $g(z_+(t_1) - (2\varphi_+ - 1)t_1)$ about $z = z_+(t_1) - (\varphi_+ + \varphi_- - 1)t_1$ completes the argument:

$$x^+(t, t_1, \varphi_+) - x_s(\varphi_+, t, z_0) = \frac{1}{2}(\varphi_- - \varphi_+)t_1^2 - \frac{1}{2}g''(\xi)(\varphi_- - \varphi_+)t_1^2,$$

for some $\xi \in (z_+(t_1) - (\varphi_+ + \varphi_- - 1)t_1, (2\varphi_+ - 1)t_1)$. But $g''(\xi) < 0$ for $\xi > 0$, and $\varphi_- > \varphi_+$, so that $x^+(t, t_1, \varphi_+) - x_s(\varphi_+, t, z_0) > 0$. This completes the proof. ■

In Fig. 4.2, we show the characteristics $C_\varphi(t)$ in the mixing zone $\mathcal{M}_1(t)$ and the contours $S_{\varphi_\pm}(t)$ (labeled $S(t;\varphi_\pm)$ in the figure) evolved from the initial interface. The evolved shock $S_E(t)$ is the same as the curve $S_\varphi(t)$, with $\varphi = \frac{1}{2}(\varphi_+ + \varphi_-)$; in the figure, the stable and unstable portions are shown. Note that the x and z scales have been expanded in order to visualize the computed solution.

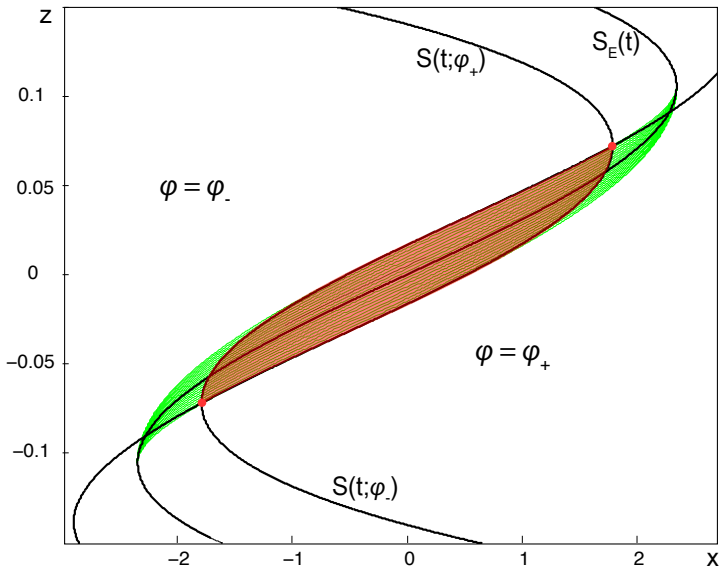

Figure 4.2: The mixing zone contains the shaded region bounded by the curves $S(t;\varphi_-)$ and $S(t;\varphi_+)$. The calculation for the figure has $\varphi_+ = 0, \varphi_- = 1$.

Breakdown of the smooth mixing solution.

The smooth mixing solution depends on $z^+(t, t_1, \varphi)$ being an increasing function of t_1, and correspondingly, $z^-(t, t_1, \varphi)$ being decreasing in t_1. In fact, when $z^+(t, t_1, \varphi)$ becomes a decreasing function of t_1, the characteristics C_ϕ overlap the evolved interface, leading to a multivalued function. In such a circumstance, there is an interaction between the characteristics and the evolved shock, leading to a structure in which there is a shock wave with non-constant φ on one side. In general, the smooth mixing solution becomes singular in this way after a finite time.

Without loss of generality, we restrict attention for now to the solution near $P_+(t)$; a similar calculation

can be carried out near $P_-(t)$. From (4.14), we find

$$\frac{\partial z^+}{\partial t_1}(t, t_1, \varphi) = -(2\varphi - 1) + z'_+(t_1). \tag{4.17}$$

Differentiating again, we have

$$\frac{\partial^2 z^+}{\partial t_1^2}(t, t_1, \varphi) = z''_+(t_1). \tag{4.18}$$

To see that $z''_+(t_1) < 0$, we differentiate (4.11):

$$g''(z_+(t) - rt)(z'_+(t) - r) + 1 = 0. \tag{4.19}$$

Differentiating again, and using (4.11), we find

$$g'''(z_+(t) - rt)(z'_+(t) - r)^2 = tz''_+(t). \tag{4.20}$$

It now follows from $g''' < 0$ (see (4.7)) that $\dfrac{\partial^2 z^+}{\partial t_1^2}(t, t_1, \varphi) = z''_+(t_1) < 0$. Consequently,

$$\frac{\partial z^+}{\partial t_1}(t, t_1, \varphi) \geq \frac{\partial z^+}{\partial t_1}(t, t, \varphi), \quad \text{for all } t_1 \in (0, t).$$

Therefore, if a singularity develops, it corresponds to $\dfrac{\partial z^+}{\partial t_1}$ first becoming zero at $t_1 = t$, for some t. That is, the singularity occurs at $P_+(t)$. Moreover, since $\dfrac{\partial z^+}{\partial t_1}(t, t_1, \varphi)$ is decreasing as a function of φ, this must first occur at $\varphi = \varphi_-$. Thus, from (4.17), the construction breaks down in the physical domain $-1 < z < 1$ if there is a first $t = t^*$ such that

$$\frac{\partial z^+}{\partial t_1}(t^*, t^*, \varphi_-) = -(2\varphi_- - 1) + z'_+(t^*) = 0 \quad \text{and} \quad z_+(t^*) < 1. \tag{4.21}$$

Although this argument has focused on the characteristics emanating from $P_+(t)$, it is just as likely that the singularity develops first due to similar behavior at $P_-(t)$. It is also possible that $\frac{\partial z^\pm}{\partial t_1}(t, t, \varphi_\pm)$ remain non-zero as t increases, and that the construction breaks down due to $z_\pm(t)$ reaching the boundary $z = \pm 1$, at some $t = \bar{t}$, a possibility that we include in the following summary of how the smooth mixing solution breaks down.

SUMMARY: *The smooth mixing solution given by (4.14) can develop a finite time singularity in one of two ways. Either the contours given by (4.14) generate a multivalued function, or $P_\pm(t)$ reaches the boundary $z = \pm 1$.*

To characterize this breakdown of the smooth mixing solution further, we formulate equations for the breakdown time. Without loss of generality, we consider the upper part of the construction (4.14). Recall that $\varphi_- > \varphi_+$ are constants in the initial condition (4.6). Let t^* denote the first time the smooth mixing solution develops a singularity. Then $z'_+(t^*) = 2\varphi_- - 1$ from (4.21), and (4.19) becomes

$$g''(z_+ - rt) = -\frac{1}{\varphi_- - \varphi_+}, \tag{4.22}$$

(where we have used $r = \varphi_+ + \varphi_- - 1$). The assumption (4.7) that $g'''(z) < 0$, implies $g''(z)$ is a decreasing function of z. Consequently, either

(1) There exists a $t = t^*$ such that $g''(z_+(t^*) - rt^*) = -\dfrac{1}{\varphi_- - \varphi_+}$ and $z_+(t^*) < 1$, or

(2) $g''(z_+(t) - rt) > -\dfrac{1}{\varphi_- - \varphi_+}$ for all $t > 0$ such that $z_+(t) \leq 1$, in which case there may be a time $t = \bar{t}$ with $z_+(\bar{t}) = 1$. In this case, a shock develops as a reflection off the boundary $z = 1$.

Examples.

1. Cubic interface.

To study cases (1) and (2) above further, we look at the example in which the initial interface is a pure cubic

$$g(z) = -kz^3, \quad \text{with } k > 0.$$

The goal here is to describe regions of parameter values $(\varphi_-, \varphi_+, k)$ for which the smooth mixing solution breaks down at $t = t^*$, and parameter values for which the breakdown is at $t = \bar{t}$. The calculation is simplified somewhat by the observation that the initial value problem is symmetric about $z = 0$. With $g(z) = -kz^3$, equation (4.22) for $t = t^*$ becomes

$$-6k(z_+(t) - rt) = -\frac{1}{\varphi_- - \varphi_+}, \tag{4.23}$$

so that $z_+(t^*) = \dfrac{1}{6k(\varphi_- - \varphi_+)} + rt^*$. Substituting $z_+(t^*)$ back into (4.11), and solving for t^* we find

$$t^* = \frac{1}{12k(\varphi_- - \varphi_+)^2}.$$

Then $t^* > \bar{t}$, when $z_+(t^*) < 1$, for which $\varphi_+ + \varphi_- - 1 < 12k(\varphi_- - \varphi_+)^2 - 2(\varphi_- - \varphi_+)$. The boundary case (i.e., $t^* = \bar{t}$) yields the inequality

$$\varphi_+ + \varphi_- - 1 < 12k(\varphi_- - \varphi_+)^2 - 2(\varphi_- - \varphi_+). \tag{4.24}$$

This is a quadratic inequality in $(\varphi_- - \varphi_+)$ and $(\varphi_- + \varphi_+)$ with $0 \leq \varphi_+ < \varphi_- \leq 1$. In Fig. 4.3, we identify three different cases for how the boundary parabola sits in the triangle $0 < \varphi_+ < \varphi_- < 1$. In each case, if (φ_-, φ_+) lies in the region labeled I, then a shock develops in the interior of the domain, whereas if (φ_-, φ_+) lies in the region labeled B, then $P_\pm$ reaches the boundary $z = \pm 1$ before the interior shock has formed. In particular, since $z_\pm(t)$ are monotonically increasing and decreasing (respectively), $P_\pm(t)$ reach the boundary in finite time, so a singularity in the mixing zone solution always develops in finite time, whether or not a singularity develops in the interior before $P_\pm(t)$ reaches the boundary.

In the special case $\varphi_- = 1, \varphi_+ = 0$ and $g(z) = -kz^3$, for $k > \dfrac{1}{6}$ the smooth mixing solution has a breakdown time of $t^* = \dfrac{1}{12k}$, when $P_\pm(t)$ reaches the boundary. If $0 < k < \dfrac{1}{6}$, then the breakdown occurs in the interior, and the time is $t = \bar{t} = 3k$. Note that for $k = \dfrac{1}{6}$, $t^* = \bar{t} = \dfrac{1}{2}$.

2. Quadratic interface.

We now consider (3.7) with an initial condition given by (4.6) where $g(z) = -\text{sgn}(z)kz^2$, with $k > 0$:

$$\varphi(x, z, 0) = \varphi_0(x, z) = \begin{cases} \varphi_-, & \text{if} \quad x < g(z), \\ \\ \varphi_+, & \text{if} \quad x > g(z). \end{cases} \tag{4.25}$$

The initial interface is vertical at the origin, so that the evolved interface has an unstable section that is replaced by a mixing zone. In the quadratic case, the smooth mixing solution is valid only for small values of k, and it never breaks down. For larger values of k, the structure of the solution is more complicated, immediately involving shocks and rarefaction waves whose precise locations depend on each another.

As the system begins to evolve, the bulk velocity introduces shear into the system, and the interface evolves according to

$$x(z, t) = zt - \text{sgn}(z)kz^2. \tag{4.26}$$

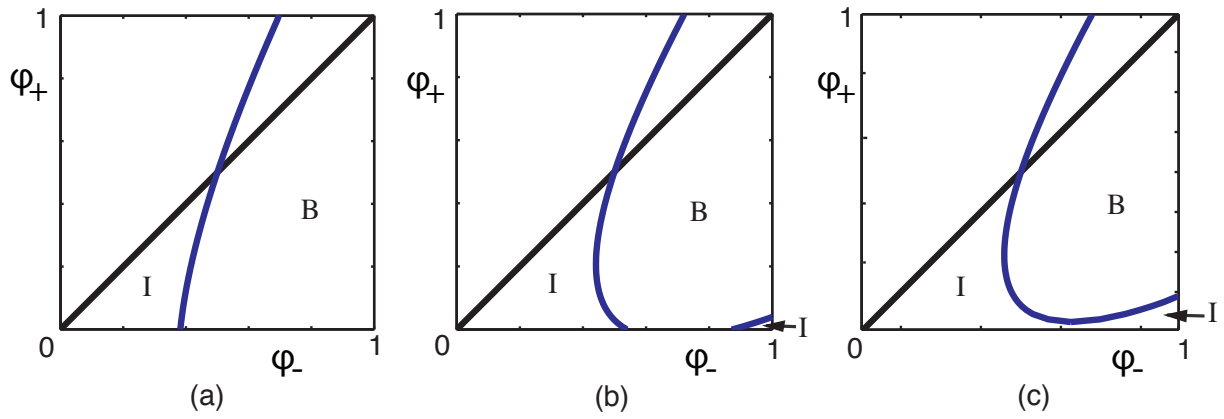

Figure 4.3: Cubic Case: dependence on k. B: shock forms at the boundary; I: shock forms in the interior.

The extrema $P_\pm(t)$ of these curves are given by

$$P_\pm(t): \quad x_\pm(t) = \pm\frac{1}{4k}t^2; \quad z_\pm(t) = \pm\frac{1}{2k}t. \tag{4.27}$$

Therefore, the points lie on the line $L(t)$:

$$L(t): \qquad x = \frac{t}{2}z. \tag{4.28}$$

Thus, the characteristics

$$C^\pm_\varphi(t): \quad \begin{cases} x^+(t,t_1,\varphi) = \dfrac{1}{2}(2\varphi-1)(t-t_1)^2 + \dfrac{1}{2k}t_1(t-t_1) + \dfrac{1}{4k}t_1^2 \\ \\ z^+(t,t_1,\varphi) = S(2\varphi-1)(t-t_1) + \dfrac{1}{2k}t_1, \qquad 0 \le t_1 \le t, \end{cases} \tag{4.29}$$

begin (with $t_1 = t$) and end (with $t_1 = 0$) on $L(t)$.

To check whether the smooth mixing solution with these contours is valid, we have only to check the sign of $\dfrac{\partial z}{\partial t_1}$ at $P_\pm(t)$, i.e, at $t_1 = t$. From (4.29) we calculate

$$\left.\frac{\partial z}{\partial t_1}\right|_{t_1=t} = -(2\varphi-1) + \frac{1}{2k}. \tag{4.30}$$

For initial condition (4.25), this quantity is smallest for $\varphi = \varphi_-$. Consequently, for $\varphi_- > \frac{1}{2}$, the mixing zone persists indefinitely if

$$k < \frac{1}{2(2\varphi_- - 1)}. \tag{4.31}$$

For example, for $\varphi_- = 1$, we have persistence of the smooth mixing zone if $k < \frac{1}{2}$. On the other hand, if (4.31) is violated, then a shock appears immediately. The case where (4.31) holds is shown in Fig 4.4.

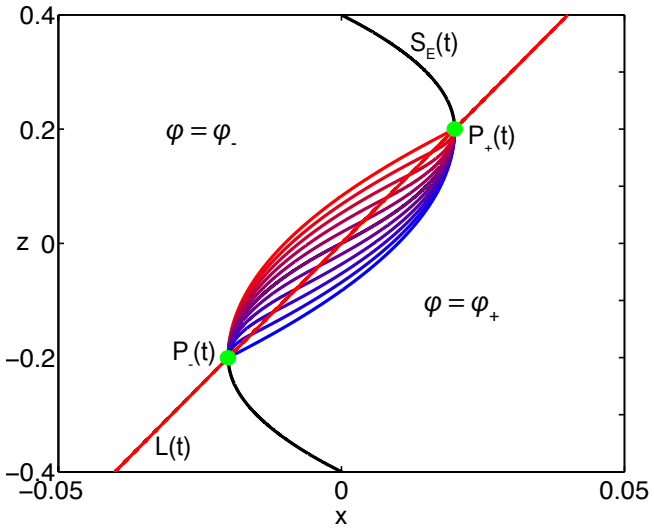

Figure 4.4: Quadratic Case: $k = \frac{1}{4}, \varphi_+ = 0, \varphi_- = 1, t = 0.1$

5 Later stages

The mixing zone $\mathcal{M}_1(t)$ constructed in §4.1 remains valid until a time $t = t^*$ characterized in equation (4.21). For $t > t^*$, the construction of $\mathcal{M}_1(t)$ breaks down. More specifically, the characteristic surfaces begin to cross near $P_\pm(t)$, generating a multi-valued solution. Consequently, the weak solution must include additional shocks, with φ non-constant on one side. In this section, we describe a numerical construction of the solution, and identify two stages in which the structure of the solution is slightly different. The latter stage persists until the domain boundary impinges on the structure of the solution.

In Figure 5.1 we show the structure of the solution for $t > t^*$ close to t^*, computed using MATLAB. We refer to this solution $\mathcal{M}_2(t)$. It is constructed from the solution $\mathcal{M}_1(t^*)$ at $t = t^*$ by using characteristics and shock fitting. Referring to Figure 5.1(b), the difficulty is that both the shock $S_I(t)$ and the solution φ in regions $\Phi_S(t)$ and $\Phi_P(t)$ evolve together: to construct $S_I(t)$, we need to know $\varphi(x, z, t_1)$ in $\Phi_S(t_1)$ for each $t^* < t_1 < t$, but this in turn depends on $S_I(t_1)$. Similarly, $\varphi(x, z, t)$ in region $\Phi_P(t)$ depends on the locations $P_+(t_1)$, forming the end points of $S_I(t_1)$ with $t^* < t_1 < t$.

We define $L_1(t)$ to be the line given by (4.14) with $t_1 = t^*$. To the left of $L_1(t)$ the contours in the region $\Phi_*(t)$ are evolved from $\mathcal{M}_1(t^*)$. That is, for each (x_0, z_0) in $\mathcal{M}_1(t^*)$, the characteristics (2.6) give the contours in $\Phi_*(t)$ parametrically. However, $\varphi = \tilde{\varphi}(x, z, t)$ is then known only implicitly in this region, and has to be found as needed by eliminating the parameter t_0 in equations (2.6). The shock $S_K(t) : x = x_K(z, t)$ is then determined numerically using the method of characteristics to solve equation (4.2), with initial condition

$$x(t_2; t_2) = x_Q(t_2) \quad z(t_2; t_2) = z_Q(t_2) \tag{5.1}$$

where $\varphi_- = \tilde{\varphi}(x_K(t)-, z, t)$ is calculated by root finding in $\Phi_*(t)$. The shock $S_K(t)$ is calculated this way until it meets $L_1(t)$, where $\varphi = \varphi_F(t)$, the value of $\varphi(x, z, t)$ corresponding to the contour that passes through the point of intersection of S_K with the line $L_1(t)$.

The shock $S_K(t)$ continues across $L_1(t)$ as $S_I(t)$, but in order to calculate it from equation (4.2), we need to know φ_- in region Φ_P. To find φ_-, we first note that the construction $\mathcal{M}_2(t)$ given in Figure 5.1 remains

valid until some time $t = \hat{t} > t^*$. This time is determined by solving (4.10) and replacing z with z^+ from (4.14) with $t_1 = 0$ and $\varphi = \varphi_+$, which in the cubic interface example from §4.1 is $\hat{t} = \dfrac{1}{2k}$. The strategy is to compute $S_I(t)$ over n small intervals $[t_j, t_j + dt]$ with $j = 0, \ldots, n-1$ where $t_j = t^* + jdt$, $t_0 = t^*$, and $dt = (\hat{t} - t^*)/n$.

In the region Φ_P, φ is approximated over N subintervals $[t_j + k\delta t, t_j + (k+1)\delta t]$ with $k = 0, \ldots, N-1$ where $\delta t = dt/N$. Since the construction is similar for each j, we will only describe it for $j = 0$. First, let $(x_0, z_0) \in S_E(t^*)$ and evolve these characteristics to get $\varphi = \varphi(x, z, t)$ given implicitly by (4.16) near $L_1(t)$. It should be noted that the transition of φ from Φ_P to $\Phi_*(t)$ is continuous across $L_1(t)$ and the contours are C^1.

We can now construct $S_I(t)$ for $t^* < t < t^* + \delta t$ from (4.2) with φ_+ constant and $\varphi_- = \varphi(x_I(z, \bar{t})-, z, t)$. $S_I(t)$ can be numerically computed to any desired accuracy with an ODE solver. We then find the point $P_+(t)$, the end point of $S_I(t)$, by finding where $\dfrac{\partial x_I}{\partial z} = 0$. We repeat this process of calculating $S_I(t)$ and finding $P_+(t)$ on the intervals $[t^* + k\delta t, t^* + (k+1)\delta t]$ until $k = N-1$. At this point, we have $P_+(t^* + k\delta t)$ for each $k = 0, \ldots, N-1$ which lets us compute φ in the regions $\Phi_P(t^* + dt)$ and $\Phi_S(t^* + dt)$ from equation (4.14) using these calculated values of $P_+(t)$ and interpolating between them. In particular, the contour $C_{\varphi_+}(t)$ terminates on $L(t)$ at a point labeled $R_-(t)$ in the figure.

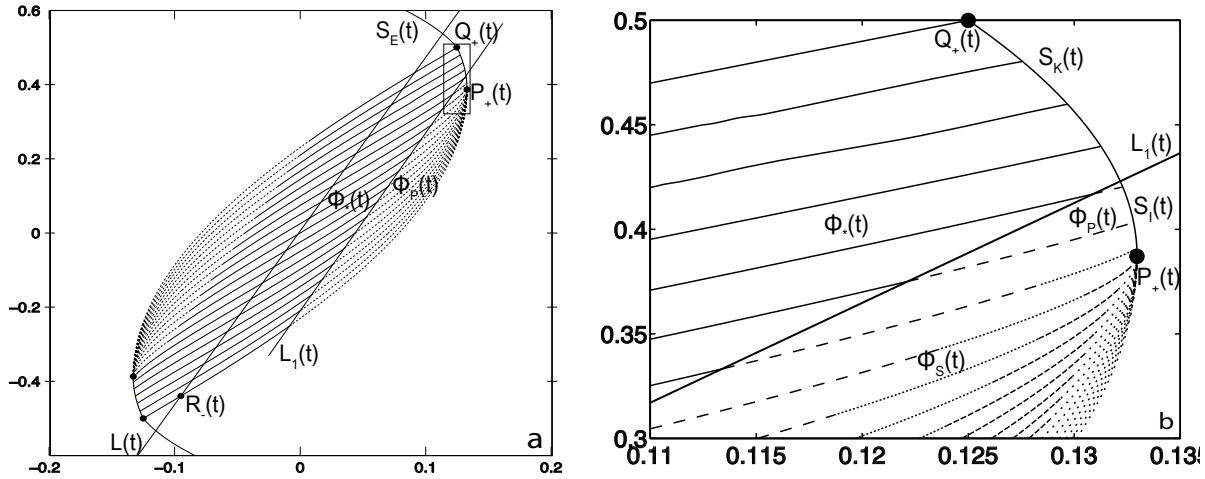

Figure 5.1: Cubic case: (a) The solution for $\mathcal{M}_2(t)$ with $n = 4, N = 61, t = \frac{1}{2k}$. (b) Zoomed in around $P_+(t)$ showing the intermediate steps used in calculating $S_I(t)$, $\Phi_S(t)$, and $\Phi_P(t)$

We now have the complete construction of $\mathcal{M}_2(t)$ at the time $t = t^* + dt$ and can repeat this process for each $t = t^* + jdt$.

This will take us up to the time $\hat{t}$ where the construction once again changes. At this time $t = \hat{t}$, the point $Q_\pm(\hat{t})$ is located on the line $L(\hat{t})$ providing a continuous location for $Q_\pm(t)$ from $\mathcal{M}_2(t)$ to $\mathcal{M}_3(t)$. As seen in Figure 5.2, the location of $Q_\pm(t)$ is where the $\varphi_\mp$ contour intersects $S_E(t)$, which now occurs when

$$x = g(z) + zt \tag{5.2}$$

with x and z given by (4.14) for some $0 < t_1 < t$. To find this exact value, we just solve (5.2) for $t_1(t) > 0$ and plug back into (4.14), giving us the point $Q_\pm(t) = \big(x_{Q_\pm}(t), z_{Q_\pm}(t)\big)$. This can be done exactly, provided the point of intersection between $S_E(t)$ and $\varphi_\mp$ falls within the $\Phi_*(t)$ region, since these contours are the known evolution of the exact solution given in $\mathcal{M}_1(t)$.

However, at a time $t = T$, the $\varphi_\pm$ contour intersects $S_E(t)$ at the line $L_1(t)$, where the solution has been numerically calculated in $\mathcal{M}_2(t)$, putting the contour in the $\Phi_S(t)$ region. Here, we can label the points in the φ_+ (and similarly for φ_-) contour $(x_i(t), z_i(t))$ with $i = 0, \ldots, (nN) - 1$. To find the point $Q_-(t)$, we simply rewrite (5.2) as

$$q_i(t) = x_i(t) - g(z_i(t)) - z_i(t)t \tag{5.3}$$

and find the first value of i for which $q_i(t)q_{i+1}(t) < 0$. We then interpolate linearly between the two points $(x_i(t), z_i(t))$ and $(x_{i+1}(t), z_{i+1}(t))$ to give us $Q_-(t)$. From here, the shock is calculated using the same procedure as in $\mathcal{M}_2(t)$, the only difference being the new location of $Q_\pm(t)$.

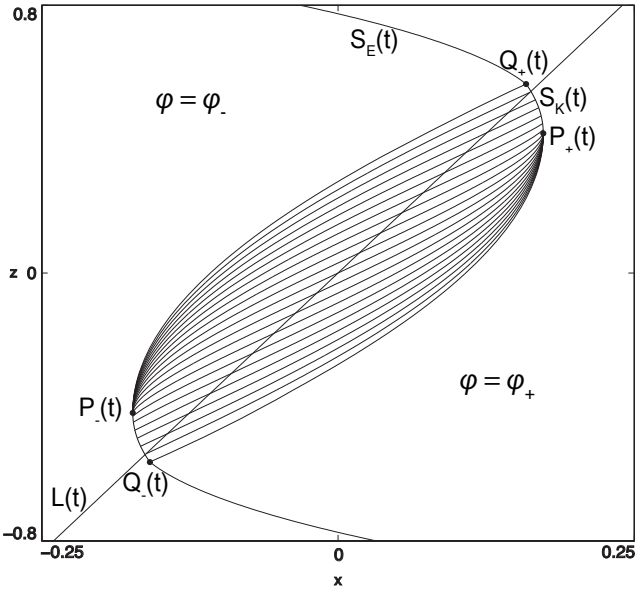

Figure 5.2: Cubic case: The solution $\mathcal{M}_3(t)$. Note, the location of $Q_\pm(t)$ is different from $\mathcal{M}_2(t)$, since the outermost contours $C_{\varphi_\pm}$ have now reached the evolved initial interface before reaching the line $L(t)$ where $t_1 = 0$.

6 Summary

In this paper, we have examined fundamental properties of the Gray-Thornton PDE model of size-segregation of granular materials in shear flow. The main results, on shock formation and shock breaking, are quite different from standard results in scalar conservation laws. Shock formation is characterized completely, due to the fortuitous structure of the equation, in which the depth-dependent velocity is a linear function. For nonlinear functions, such as for the exponential depth dependence considered in [8], shock formation is much more subtle, and only partial results are available [13]. It is well known that shock waves can break, thereby losing stability. The resulting structure is examined in detail in this paper, using an analytic construction for short time. After the short-time solution breaks down, a numerical method is needed, based on the analysis of rarefactions and shocks for the equation. The rarefaction waves appear as curves of contours of the solution, emanating from a pair of points that evolve with the solution. The rarefactions also interact dynamically with a pair of shock waves. The entire structure represents a mixing zone through which small

and large particles are transported; it replaces what would be an unstable portion of the shock wave evolved directly from the point of breaking of the original wave. The computed solution persists until the top and bottom of the mixing zone reaches the boundary.

Acknowledgments

The authors are grateful to Karen Daniels, Lindsay May and Nico Gray for helpful conversations and suggestions. This research was supported by the National Science Foundation under grants DMS-0604047 and DMS-0636590.

References

[1] E. D. Conway. The formation and decay of shocks for a conservation law in several dimensions. *Arch. Rat. Mech. Anal.*, 64:47–57, 1977.

[2] J.M.N.T. Gray and V.A. Chugunov . Particle-size segregation and diffusive remixing in shallow granular avalanches. J. Fluid Mech. 569 , 365-398, 2006.

[3] J. M. N. T. Gray, M. Shearer, and A. R. Thornton. Time-dependent solutions for particle-size segregation in shallow granular avalanches. *Proc. Roy. Soc. A*, 462(2067):947–972, 2006.

[4] J.M.N.T. Gray and A.R. Thornton. A theory for particle size segregation in shallow granular free-surface flows. *Proc. Roy. Soc. A*, 461:1447–1473, 2005.

[5] F. John. Formation of singularities in one-dimensional nonlinear wave propagation. *Comm. Pure Appl. Math.*, 27:377–405, 1974.

[6] P. D. Lax. Hyperbolic systems of conservation laws II. *Comm. Pure Appl. Math.*, 10:537–566, 1957.

[7] A. Majda. *Compressible Fluid Flow and Systems of Conservation Laws in several Space Dimensions*, volume 53. Springer-Verlag, 1984.

[8] L. B. H. May, M. Shearer, and K. E. Daniels. Scalar conservation laws with nonconstant coefficients with application to particle size segregation in granular flow. 2009. Submitted to J. Nonlinear Science.

[9] M. McIntyre, E. L. Rowe, M. Shearer, J. M. N. T. Gray, and A. R. Thornton. Evolution of a Mixing Zone in Granular Avalanches. *Appl Math Res Express*, 2007(abm008):abm008–12, 2007.

[10] S.B. Savage and C.K.K. Lun. Particle size segregation in inclined chute flow of dry cohesionless granular solids. *J. Fluid Mech.*, 189:311–335, 1988.

[11] D. Serre. *Systems of Conservation Laws: Geometric structures, oscillations, and initial-boundary value problems*. Cambridge Univ. Press, 2000.

[12] M. Shearer, J.M.N.T. Gray, and A.R. Thornton. Stable solutions of a scalar conservation law for particle size segregation in dense granular avalanches. *European J. Applied Math.*, 19:61–86, 2008.

[13] M. Shearer, L.B.H. May, N. Giffen and K.E. Daniels, The Gray-Thornton model of granular segregation. Joint IUTAM-ISIMM Symposium on Mathematical Modeling and Physical Instances of Granular Flows. Submitted 2009.

[14] A. R. Thornton and J. M. N. T. Gray. Breaking size segregation waves and particle recirculation in granular avalanches. *J. Fluid Mech.*, 596:261–284, 2008.